RSC Advances

PAPER

View Article Online
View Journal | View Issue

Cite this: *RSC Adv.*, 2025, **15**, 4458

2-Amino-4,6-diarylpyrimidines as potential chronic myeloid leukemia cell inhibitors targeting anti-ABL1 kinase: microwave-assisted synthesis, biological evaluation, molecular docking, and dynamics studies†

Thi-Anh-Truc Phan,[ab] Kim-Khanh-Huy Ngo,[a] Thi-Cam-Thu Nguyen,[a] Thanh-Tan Mai,[c] Hai-Dang Nguyen,[d] Thu-Trang Duong,[d] Le-Phu Tran,[ab] Thanh-Tuyen Duong,[ab] Thi-Kim-Chi Huynh,[a] Elena V. Koroleva,[e] Zhanna V. Ignatovich,[e] Anastasiya L. Ermolinskaya,[e] Hoang-Phuc Nguyen,[a] Thi-Hong-An Nguyen,[a] Anh-Khoa Ton,[a] Tuong-Ha Do[b] and Thi-Kim-Dung Hoang *[a]

In this work, a simple and mild process was used to synthesize a series of 2-amino-4,6-diarylpyrimidine derivatives, **1a–1q**, whose structures were verified by FTIR, 1D- and 2D-NMR, and HRMS techniques, to investigate and develop anticancer agents. Under microwave irradiation, a two-step process was carried out, consisting of aldol condensation of benzaldehydes and acetophenones to produce intermediate chalcones and ring closure condensation of chalcones and guanidine hydrochloride. Each generated compound's anticancer activity against the human chronic myelocytic leukemia K562 cancer cell line was investigated *in vitro* to determine the active compounds, which were subsequently evaluated for inhibiting the ABL1 tyrosine kinase. According to these findings, compound **1e** demonstrated considerable inhibition against K562 cancer cells and ABL1 tyrosine kinase at IC_{50} values of 8.77 ± 0.55 μM and 3.35 ± 0.58 μM, respectively. The molecular docking on wild-type and mutant type ABL1 (PDB ID 2HYY and 5MO4) investigation indicated that **1e** and **1g** interacted with amino acids. It formed stable hydrogen bonds and π–π linkages with crucial residues in the active site of the enzyme. Moreover, the stability of these enzyme–ligand complexes was confirmed using molecular dynamics simulations. These findings suggested that compounds **1e** and **1g** can be considered promising cancer treatment agents.

Received 24th November 2024
Accepted 27th January 2025

DOI: 10.1039/d4ra08330j

rsc.li/rsc-advances

1. Introduction

Cancer remains a formidable challenge for global health, standing as one of the major causes of death worldwide.[1,2] The World Health Organization reports that roughly 14 million new cancer cases are diagnosed annually, resulting in around 9 million deaths.[3] Among the diverse spectrum of cancer types, leukemia, which is defined by the malignant expansion of hematopoietic stem cells in the bone marrow, occupies a significant position due to its prevalence and clinical complexity.[4,5] Notably, human chronic myeloid leukemia (CML) represents a subset of leukemia distinguished by the aberrant expansion of myeloid progenitor cells.[6,7] Since the discovery of the presence of a unique and constant chromosomal abnormality more than four decades ago, significant achievements have been made in understanding the biological underpinnings of the disease.[8,9] In leukemia research, the K562 cell line has emerged as a cornerstone for investigating the pathogenesis and therapeutic strategies pertinent to CML.[10,11]

Tyrosine kinases (TKs) are the enzymes that initiate the transfer of phosphate groups from ATP to tyrosine, a vital process in cellular machinery. The K562 cell line, which expresses the BCR-ABL fusion gene, was discovered to be exceptionally resistant to apoptosis, regardless of the triggering

[a]*Institute of Chemical Technology, Vietnam Academy of Science and Technology, No. 1A, TL29 St., Thanh Loc Ward, Dist. 12, Ho Chi Minh City 70000, Vietnam. E-mail: hoangthikimdung@gmail.com; htkdung@ict.vast.vn*

[b]*Ton Duc Thang University, No. 19, Nguyen Huu Tho St., Tan Hung Ward, Dist. 7, Ho Chi Minh City 70000, Vietnam*

[c]*University of Medicine and Pharmacy at Ho Chi Minh City, No. 41, Dinh Tien Hoang St., Ben Nghe Ward, Dist. 1, Ho Chi Minh City 70000, Vietnam*

[d]*University of Science and Technology of Hanoi, Vietnam Academy of Science and Technology, No. 18, Hoang Quoc Viet St., Nghia Do Ward, Cau Giay District, Ha Noi City 100000, Vietnam*

[e]*Institute of Chemistry of New Materials, National Academy of Sciences of Belarus, 36, F. Skorina St., Minsk, 220141, Republic of Belarus*

† Electronic supplementary information (ESI) available. See DOI: https://doi.org/10.1039/d4ra08330j

stimulus, and scientists clarified the role of the BCR-ABL fusion protein and the Philadelphia chromosome in CML pathogenesis.[12,13] Therefore, BCR-ABL inhibition is currently viewed as a significant molecular target in the treatment of CML. Imatinib and nilotinib (commercially known as Glivec and Tasigna, respectively) are kinase inhibitors that have emerged as a primary therapeutic agent for CML cancer treatment and represents a cornerstone of contemporary anticancer pharmacotherapy.[14,15] Nonetheless, imatinib resistance linked to BCR/ABL1 mutation and the common adverse effects of marketed drug have emerged as a problem.[16–18] Therefore, developing potential inhibitors with improved medication safety and efficacy is critical for treating CML patients. Recent reports have revealed that the structure of imatinib, nilotinib and their derivatives containing pyrimidine-2-amine showed inhibitory potential through the kinase pathway (Fig. 1).[14,19,20] Additionally, different types of substituents linked to the C-4 and C-6 positions of pyrimidine-2-amine were found to have antiproliferative effects on diverse cell lines.[21–24] This has led to our current research focusing on the synthesis of a pyrimidine-2-amine skeleton containing aryl substituents at the 4,6-position of the pyrimidine backbone, as well as the investigation of K562 cell line and ABL1 tyrosine kinase inhibitory activities.

With the importance and extensive range of biological activities associated with pyrimidine moieties, numerous methods for pyrimidine synthesis have been reported.[25,26] Pyrimidine nucleus production is classified into three kinds according to the fundamental structure of the reactants combining (Fig. S1†), with type 1 being considered the most prevalent pyrimidine synthesis method.[27] Chalcones are the most popular and highly stable precursors in the synthesis of numerous biologically active pyrimidines based on type 1 (ref. 28–30) because they could easily react with guanidine salts in basic conditions to produce 2-amino-4,6-diarylpyrimidines.[31–34]

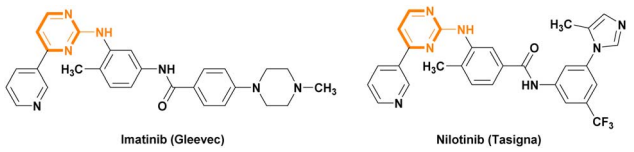

Fig. 1 Structures of commercial anticancer drugs containing pyrimidin-2-amine moiety.

2. Results and discussion

2.1. Chemistry

The target 2-amino-4,6-diarylpyrimidines **1a–1q** were synthesized following the approach illustrated in Scheme 1. The one-pot method was attempted to cyclocondense the three-components among benzaldehydes, acetophenones, and guanidine hydrochloride (GHCl), but the results were not considered due to the excessive amount of impurities. Consequently, the synthesis procedure of the desired compounds was separated into two steps, which was carried out by utilizing the microwave (MW) technique. The intermediate chalcones were generated in the first stage using aldol condensation of substituted benzaldehyde and various acetophenone derivatives in ethylene glycol (EG) solvent with KOH catalysis *via* MW (80 °C, 100 W, 10–30 min). The second step of this work involved ring closure condensation of pure substituted chalcones, GHCl, and NaOH in pyridine under MW conditions (100 °C, 180 W, 5–10 min). The final compounds were produced with a yield ranging from 31% to 64% (Table 1) and the synthesis of pyrimidines that contained electron-withdrawing groups was listed in Table S1.† EG was utilized as a recyclable, non-volatile, and cost-effective solvent to efficiently dissolve reactants in the chalcone synthesis. This work-up procedure was convenient,

Table 1 Structure of 2-amino-4,6-diarylpyrimidines **1a–1q** with various substituted groups and their yields

Entry	Products	R_1	R_2	Yield (%)
1	**1a**	2′-OH	H	41
2	**1b**	2′-OH	2″-OH	51
3	**1c**	2′-OH	3″-OCH_3	56
4	**1d**	2′-OH	4″-OCH_3	43
5	**1e**	2′-OH	4″-Br	33
6	**1f**	2′-OH	4″-Cl	31
7	**1g**	3′-OCH_3	H	36
8	**1h**	3′-OCH_3	4″-OH	48
9	**1i**	3′-OCH_3	4″-OCH_3	45
10	**1j**	3′-OCH_3	4″-Br	55
11	**1k**	3′-OCH_3	4″-Cl	48
12	**1l**	4′-OCH_3	H	47
13	**1m**	4′-OCH_3	4″-OH	42
14	**1n**	4′-OCH_3	4″-OCH_3	33
15	**1o**	4′-OCH_3	4″-Br	48
16	**1p**	4′-OCH_3	4″-Cl	64
17	**1q**	4′-OH	H	44

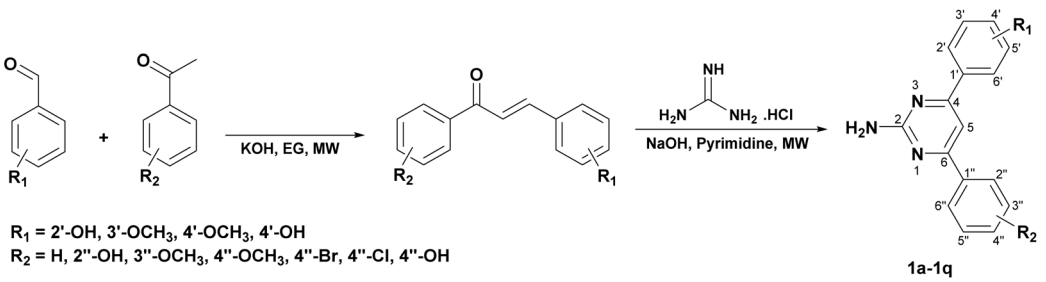

Scheme 1 Synthesis process of 2-amino-4,6-diarylpyrimidine derivatives **1a–1q**.

Table 2 Compound **1h**'s ^{1}H and ^{13}C-NMR spectra, and HSQC and HMBC correlations

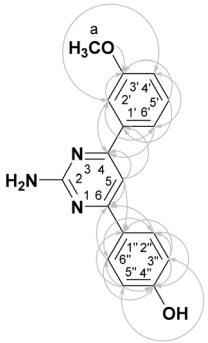

Position	^{1}H-NMR (ppm)	^{13}C-NMR (ppm)	Correlations	
			HSQC	HMBC
2	—	163.78	—	—
4	—	164.12	—	—
5	7.57 (1H, s)	100.93	C-5	C-4, C-6, C-1′, C-1″
6	—	164.68	—	—
1′	—	139.08	—	—
2′	7.72 (1H, s)	112.00	C-2′	C-4, C-3′, C-4′, C-6′
3′	—	159.53	—	—
4′	7.07 (1H, dd, 2.4 Hz, 7.8 Hz)	115.95	C-4′	C-2′, C-6′
5′	7.42 (1H, t, 7.8 Hz)	129.56	C-5′	C-1′, C-3′
6′	7.77 (1H, d, 7.8 Hz)	119.26	C-6′	C-4, C-2′, C-4′
1″	—	127.99	—	—
2″	8.09 (2H, d, 9.0 Hz)	128.63	C-2″	C-6, C-4″, C-6″
3″	6.87 (2H, d, 9.0 Hz)	115.25	C-3″	C-1″, C-2″, C-4″, C-5″
4″	—	159.74	—	—
5″	6.87 (2H, d, 9.0 Hz)	115.25	C-5″	C-1″, C-3″, C-4″, C-6″
6″	8.09 (2H, d, 9.0 Hz)	128.63	C-6″	C-6, C-2″, C-4″
a	3.85 (3H, s)	55.22	C-a	C-3′
–NH_2	6.58 (2H, s)	—	—	—
–OH	9.89 (1H, s)	—	—	—

straightforward, and prompt in preparing the final product and handling the post-reaction mixture. The structures of all synthesized derivatives were demonstrated carefully by FTIR, 1D- and 2D-NMR, and ESI-HRMS analyses. The novel compound **1h** was obtained in the form of a pale brown powder. The FTIR of **1h** indicated a sharp and medium peak at 3403 cm^{-1}, which corresponded to the primary amine's N–H stretching vibration. Characteristic oscillations were also found at 3517, 1636, 1542, 1241, and 1037 cm^{-1} for the –OH, C=N, C=C, C–N, and –OCH_3 groups, respectively. Compound **1h**'s NMR spectra revealed nine aromatic protons at δ_H 6.87–8.09 ppm, corresponding to aromatic carbons at δ_C 100.93–164.12 ppm (Table 2). Additionally, the characteristic singlets at the chemical shift δ_H 3.85, 6.58, and 9.89 ppm were assigned to the protons of OCH_3, NH_2, and OH groups, respectively. This finding demonstrated the successful aldol condensation of 3-methoxybenzaldehyde with 4-acetophenone and cyclo-condensation processes of the corresponding chalcone with GHCl. The HSQC spectrum revealed the direct interaction between methyl proton at 3.85 ppm (H-a) and methyl carbon at 55.22 ppm (C-a). Then, the correlation in the HMBC spectrum was determined between aromatic protons at 7.72 ppm (H-2′), 7.77 ppm (H-6′), and 7.57 ppm (H-5) and the same quaternary carbon at 164.12 ppm (C-4), between aromatic protons at 7.57 ppm (H-5) and 8.09 ppm (H-2″/H-6), and the same carbon at 164.68 ppm (C-6). The ring closure sites at quaternary carbons C-4 and C-6 were discovered to generate compound **1h**. The molecular formula of **1h** was confirmed as $C_{17}H_{16}N_3O_2$ by ESI-HRMS analysis, showing a pseudo-molecular ion peak $[M + H]^+$ m/z 294.1249 (calcd for $C_{17}H_{16}N_3O_2$, 294.1242). On the basis of the previously given spectrum data, 4-(2-amino-6-(3-methoxyphenyl)-pyrimidin-4-yl)-phenol was identified as the structure of **1h**.

2.2. Cytotoxicity assay

Anti-proliferative activity on K562 cell line. The anti-proliferative activity of all the produced derivatives **1a–1q** was tested *in vitro* against the K562 human leukemia cell line using the MTT method, with imatinib serving as a positive control. Initially, the inhibited cell survival was assessed and expressed as CS values. The active compounds with CS values > 50% (Table S4†) were chosen for further testing. Table 3 presents the IC_{50}

Table 3 Anti-tumor activity of 2-amino-4,6-diarylpyrimidine derivatives against K562 cancer cells[a]

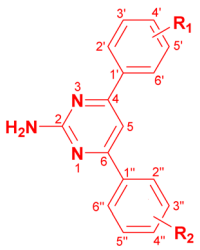

1a-1q

Entry	Compound	R_1	R_2	$IC_{50} \pm SD$ (μM)
1	**1a**	2′-OH	H	57.41 ± 1.76
2	**1b**	2′-OH	2″-OH	ND
3	**1c**	2′-OH	3″-OCH_3	82.04 ± 1.89
4	**1d**	2′-OH	4″-OCH_3	ND
5	**1e**	2′-OH	4″-Br	8.77 ± 0.55
6	**1f**	2′-OH	4-Cl	ND
7	**1g**	3′-OCH_3	H	32.43 ± 1.59
8	**1h**	3′-OCH_3	4″-OH	48.42 ± 1.81
9	**1i**	3′-OCH_3	4″-OCH_3	ND
10	**1j**	3′-OCH_3	4-Br	57.68 ± 1.73
11	**1k**	3′-OCH_3	4″-Cl	ND
12	**1l**	4′-OCH_3	H	61.94 ± 1.62
13	**1m**	4′-OCH_3	4″-OH	43.25 ± 1.42
14	**1n**	4′-OCH_3	4″-OCH_3	ND
15	**1o**	4′-OCH_3	4″-Br	ND
16	**1p**	4′-OCH_3	4″-Cl	ND
17	**1q**	4′-OH	H	ND
18	Imatinib			0.116 ± 0.002

[a] ND: not determined.

values for the inhibitory effects together with the standard deviations (±SD) derived from three separate experiments. According to the overall findings, these 17 pyrimidine derivatives have activity against the K562 cell line, but not as much as that of imatinib. The substituted groups on benzaldehyde (R_1) and acetophenone (R_2) skeletons were modified at 4- and 6-positions of the 2-aminopyrimidine skeleton, respectively, indicating their effect on the cytotoxicity activity.

When benzaldehydes and acetophenone (R_2 = H) were combined, the compounds containing 2′-hydroxy (**1a**), 3′-methoxy (**1g**), and 4′-methoxy (**1l**) groups showed moderate anti-tumor activity (IC_{50} = 32.43–61.94 μM), whereas the 4-hydroxy group (**1q**) did not. It showed good activity in the four compounds mentioned above when a molecule was attached to only the 3′-methoxy group on the benzaldehyde ring of 4-position on the pyrimidine backbone. Therefore, the inhibitory activity against K562 cell line was further investigated by immobilizing R_1 substituents (2′-hydroxy, 3′-methoxy, and 4′-methoxy) and modifying R_2 substituted groups.

Methoxy, hydroxy, and halogen (chloro and bromo) groups were bonded to 4-position on the acetophenone skeleton and demonstrated their activity when compared with compounds **1a**, **1g**, and **1l**. Unfortunately, the compounds with the methoxy group, such as **1d**, **1i**, and **1n**, completely lost their anti-tumor activity. Compounds **1h** and **1m** exhibited a moderate anti-proliferative effect in the presence of hydroxy groups, corresponding with IC_{50} values of 48.42 ± 1.81 and 43.25 ± 1.42 μM, respectively. The substitution of halogen groups such as chloro and bromo revealed a considerable variation in their bioactivity. Compounds with the chloro group (**1f**, **1k**, and **1p**) significantly decreased the inhibitory activity of compounds that contained the acetophenone ring only. Meanwhile, the presence of the bromo group (**1e** and **1i**) resulted in moderate to good activity (IC_{50} = 8.77–57.68 μM), except for compound **1o**. The anti-proliferative effect of compound **1e** was remarkably enhanced by the combination of 2′-hydroxy group on R_1 and 4″-bromo group on R_2, as evidenced by its IC_{50} value of 8.77 ± 0.55 μM. Furthermore, adding 2″-hydroxy (**1b**) and 3″-methoxy (**1c**) groups to the acetophenone ring did not improve its inhibitory effect against the K562 cancer cell line.

In the summary, these findings revealed the correlation between the structure of 2-amino-4,6-diarylpyrimidine derivatives and bioactivity against the K562 cancer cell line. The substituted benzaldehydes (3′-OCH_3, 4′-OCH_3) at C-4 pyrimidine ring were combined with different acetophenones (3″-OCH_3, 4″-OCH_3, 4″-Cl, 4″-Br) at C-6 pyrimidine ring, which significantly reduced the anti-tumor activity. Significantly, the compounds were generated by combining the 4- and 6-position substituents (3-methoxybenzaldehyde and acetophenone, 2-hydroxybenzaldehyde and 4-bromoacetophenone) of the pyrimidine ring, thereby significantly boosting the anti-proliferative activity against K562 cancer cell line. As a result, compounds **1e** and **1g** were chosen for further investigation into ABL1 tyrosine kinase inhibitory activity.

ABL1 tyrosine kinase inhibitory activities. Human erythroleukemic K562 cells, which are pseudo-triploid and positive for the Philadelphia chromosome, serve as the prototypical CML cell culture model. Thus, K562 cells have been extensively employed in studies involving the *BCR/ABL1* oncogene and the tyrosine kinase inhibitor (TKI). Tyrosine-protein kinase ABL1 (ABL1) is a non-receptor tyrosinase that plays a crucial role in regulating various cellular processes, including cell proliferation, adhesion, and apoptosis. ABL1 is involved in multiple signaling pathways, including those mediated by growth factors, cytokines, and integrins. Dysregulation of ABL1 activity has been linked to the pathogenesis of several diseases, particularly cancer, where it can promote tumorigenesis and metastasis. Patients with CML have improved their overall survival rate by using BCR-ABL TKIs, including imatinib, nilotinib, dasatinib, bosutinib, and ponatinib.[35] However, their application is limited due to drug resistance and significant

Table 4 ABL1 tyrosine kinase inhibitory activity (IC_{50}, μM) of 2-amino-4,6-diarylpyrimidine derivatives

Entry	Compound	$IC_{50} \pm SD$ (μM)
1	**1e**	3.35 ± 0.58
2	**1g**	35.16 ± 1.83
3	Imatinib	0.069 ± 0.002

side effects. Thus, finding a new source of ABL1 inhibitors is an important task in identifying promising therapeutics for the treatment of certain cancers such as CML and acute lymphoblastic leukemia.

In this investigation, the concentration of ABL1 in the sample was measured by Human ABL1 Elisa Kit (FineTest, EH4452) according to the manufacturer's protocol. As seen in Fig. S102,† a significant decrease in ABL1 production was observed for all treated compounds compared with the control ($p < 0.0001$). As we can see in Table 4, compound **1e** exhibited the strongest activity with 80% inhibition of ABL1 production at a concentration of 30 μM and IC_{50} value of 3.35 ± 0.58 μM. Compound **1g** showed the weakest inhibition with an IC_{50} value of 35.16 ± 1.83 μM. The positive control imatinib revealed a significant decrease in ABL1 production in a dose-dependent manner. A similar trend was achieved in all tested compounds.

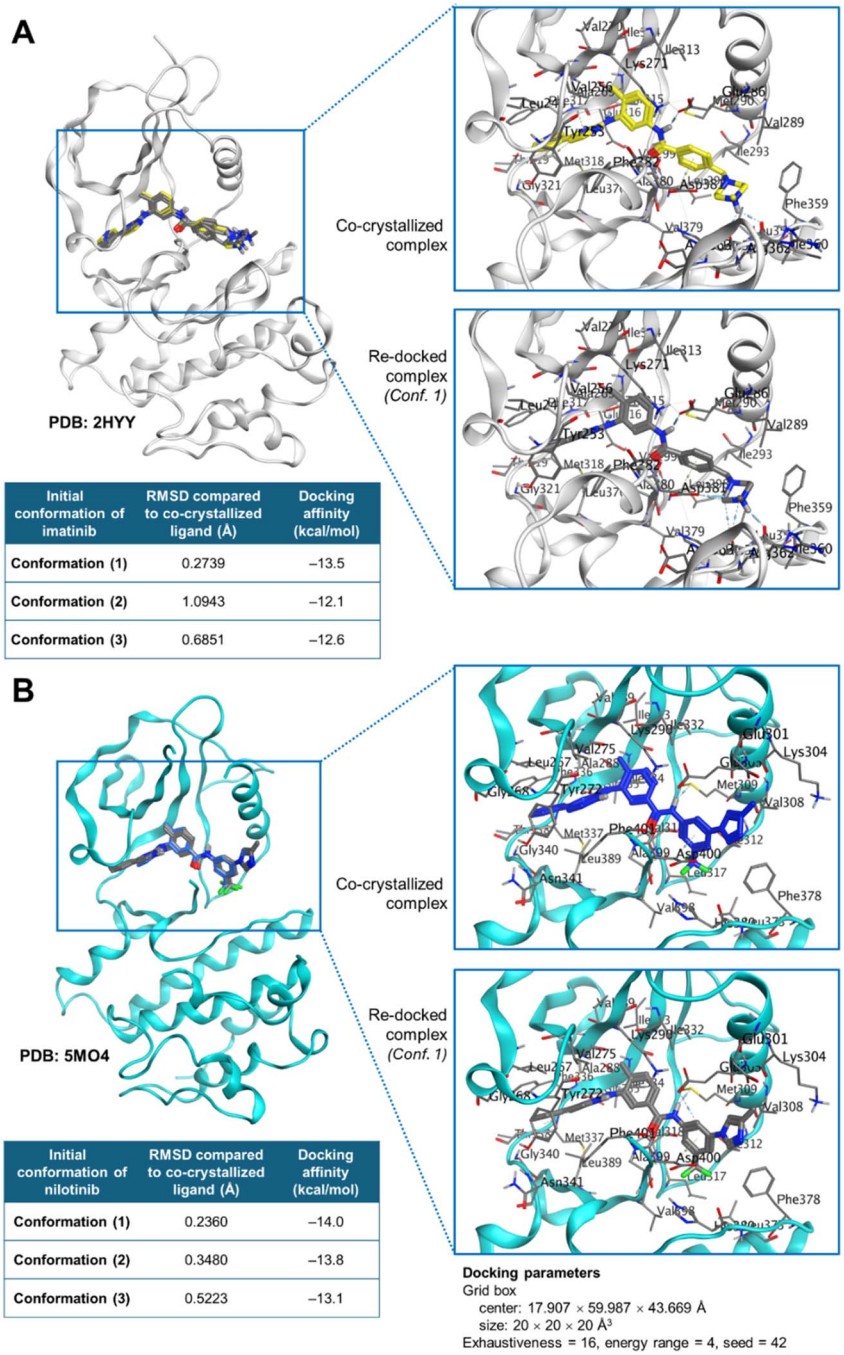

Initial conformation of imatinib	RMSD compared to co-crystallized ligand (Å)	Docking affinity (kcal/mol)
Conformation (1)	0.2739	−13.5
Conformation (2)	1.0943	−12.1
Conformation (3)	0.6851	−12.6

Initial conformation of nilotinib	RMSD compared to co-crystallized ligand (Å)	Docking affinity (kcal/mol)
Conformation (1)	0.2360	−14.0
Conformation (2)	0.3480	−13.8
Conformation (3)	0.5223	−13.1

Fig. 2 Results of redocking co-crystallized inhibitors onto ABL1 kinase. (A) Redocking of three imatinib conformations (in gray sticks) onto wild-type ABL1 showed a strong alignment with the co-crystallized ligand (in yellow sticks), with corresponding RMSD values. (B) Similarly, redocking of three nilotinib conformations (in gray sticks) onto mutant ABL1 (T334I-D382N) displayed a good match with the co-crystallized ligand (in blue sticks), along with their respective RMSD values. Zoomed-in views highlight the nearby residues and their interactions with the co-crystallized and re-docked ligands.

Table 5 Docking results of 17 2-amino-4,6-diarylpyrimidine derivatives on ABL1 (PDB ID 2HYY)[a]

Compound	IC_{50} (μM) (cell-based)	IC_{50} (μM) (enzyme)	ΔG_{vina} (kcal mol^{-1})	Interaction with ABL1WT residues
1b	—	—	−9.0	Thr315 (HBD), Glu316 (HBD, HBA), Met318 (HBD), Phe317 (π–π), Phe382 (π–π, Hyd), Leu248, Val256, Tyr253 (Hyd)
1c	82.04 ± 1.89	—	−8.8	Glu316 (HBD), Met318 (HBA), Phe317 (π–π), Phe382 (π–π, Hyd), Leu248, Tyr253, Val256 (Hyd)
1a	57.41 ± 1.76	—	−8.8	Thr315 (HBD), Met318 (HBA), Phe317 (π–π), Phe382 (π–π, Hyd), Leu248, Tyr253, Val256 (Hyd)
1e	8.77 ± 0.55	3.35 ± 0.58	−8.6	Glu286 (HBD), Ala269 (HBD, Hyd), Tyr253 (π–π), Phe382 (π–π, Hyd), Leu248, Met290, Val299 (Hyd)
1f	—	—	−8.6	Thr315 (HBD), Ala269 (HBD), Tyr253 (π–π, Hyd), Phe382 (π–π, Hyd), Leu248, Met290 (Hyd)
1g	32.43 ± 1.59	35.16 ± 1.83	−8.6	Phe317 (π–π, Hyd), Phe382 (π–π, Hyd), Leu248, Val256, Gly321 (Hyd)
1j	57.68 ± 1.73	—	−8.6	Ala269 (HBD), Tyr253 (π–π, Hyd), Phe382 (π–π, Hyd), Leu248, Met290, Leu370 (Hyd)
1o	—	—	−8.6	Ala269 (HBD, Hyd), Tyr253 (π–π), Phe382 (π–π, Hyd), Leu248, Met290, Asp381 (Hyd)
1d	—	—	−8.5	Ala269 (HBD), Thr315 (HBD), Tyr253 (π–π, Hyd), Phe382 (π–π, Hyd), Leu248, Met290, Ala380, Asp381 (Hyd)
1k	—	—	−8.5	Ala269 (HBD), Tyr253 (π–π, Hyd), Phe382 (π–π, Hyd), Leu248, Met290, Leu370 (Hyd)
1p	—	—	−8.5	Ala269 (HBD, Hyd), Tyr253 (π–π), Phe382 (π–π, Hyd), Leu248, Ala269, Met290, Asp381 (Hyd)
1i	—	—	−8.4	Ala269 (HBD, Hyd), Tyr253 (π–π), Phe382 (π–π, Hyd), Leu248, Met290, Leu370, Ala380, Asp381 (Hyd)
1n	—	—	−8.4	Ala269 (HBD, Hyd), Tyr253 (π–π), Phe382 (π–π, Hyd), Leu248, Met290, Asp381 (Hyd)
1h	48.42 ± 1.81	—	−8.3	Ala269 (HBD), Tyr253 (π–π, Hyd), Phe382 (π–π, Hyd), Leu248, Leu370, Met290 (Hyd)
1m	43.25 ± 1.42	—	−8.3	Ala269 (HBD, Hyd), Tyr253 (π–π, Hyd), Phe382 (π–π, Hyd), Leu248, Met290 (Hyd)
1q	—	—	−8.2	Thr315 (HBA), Phe317 (π–π, Hyd), Phe382 (π–π, Hyd), Leu248, Gly321 (Hyd)
1l	61.94 ± 1.62	—	−8.2	Ala269 (HBD), Tyr253 (π–π, Hyd), Phe382 (π–π, Hyd), Leu248, Ala269, Met290, Leu370, Ala380, Asp381 (Hyd)
Imatinib	0.116 ± 0.002	0.069 ± 0.002	−13.5	Glu286 (HBD), Thr315 (HBD, Hyd), Met318 (HBA), Ile360 (HBD), Asp381 (HBA, Hyd), Tyr253 (π–π, Hyd), Phe317 (π–π, Hyd), Phe382 (π–π, Hyd), Leu248, Val256, Lys271, Val289, Met290, Leu370 (Hyd)

[a] HBD: hydrogen bond donor, HBA: hydrogen bond acceptor, π–π: pi–pi stacking, Hyd: hydrophobic interaction.

On the basis of these findings, we can suggest that compound **1e** has the potential for CML prevention and treatment. Several experiments, such as apoptosis, cell cycle arrest, and western blot, need to be conducted to determine the mechanism of action of this compound.

2.3. Computational analysis

Molecular docking studies. For wild-type ABL1 kinase, the grid box was defined on the basis of the position of imatinib in the PDB 2HYY structure, with coordinates center_x = 17.907, center_y = 59.987, and center_z = 43.669, and dimensions of 20 × 20 × 20 Å^3. The redocking approach was employed to assess the accuracy of the docking protocol. Three different conformations of imatinib were used for redocking: (1) the co-crystallized conformation with ABL1, (2) the co-crystallized conformation after energy minimization, and (3) the conformation obtained from redrawing imatinib followed by energy minimization. The results, as shown in Fig. 2A, demonstrate that AutoDock Vina successfully reproduced the binding conformation of imatinib in each of the initial conformations, with RMSD values of less than 2 Å. Similarly, nilotinib was redocked to the ABL1 T334I-D382N mutant (PDB ID 5MO4) using the same grid box parameters as those for imatinib at the enzyme's active site. The results in Fig. 2B demonstrate that the docking procedure effectively reproduced the bound conformation of nilotinib, with an RMSD of less than 1 Å. Therefore, these molecular docking protocols can be reliably applied to assess the binding of the investigated compounds to both wild-type and mutant forms of ABL1.

The docking results of 17 2-amino-4,6-diarylpyrimidine derivatives on wild-type ABL1 are presented in Table 5. All investigated compounds exhibited docking affinities <−8.0 kcal mol^{-1}, which were weaker than that of imatinib (−13.5 kcal mol^{-1}). However, the docking score range of the synthesized compounds still suggested potential activity. The interaction diagrams of the best docking pose of each ligand are

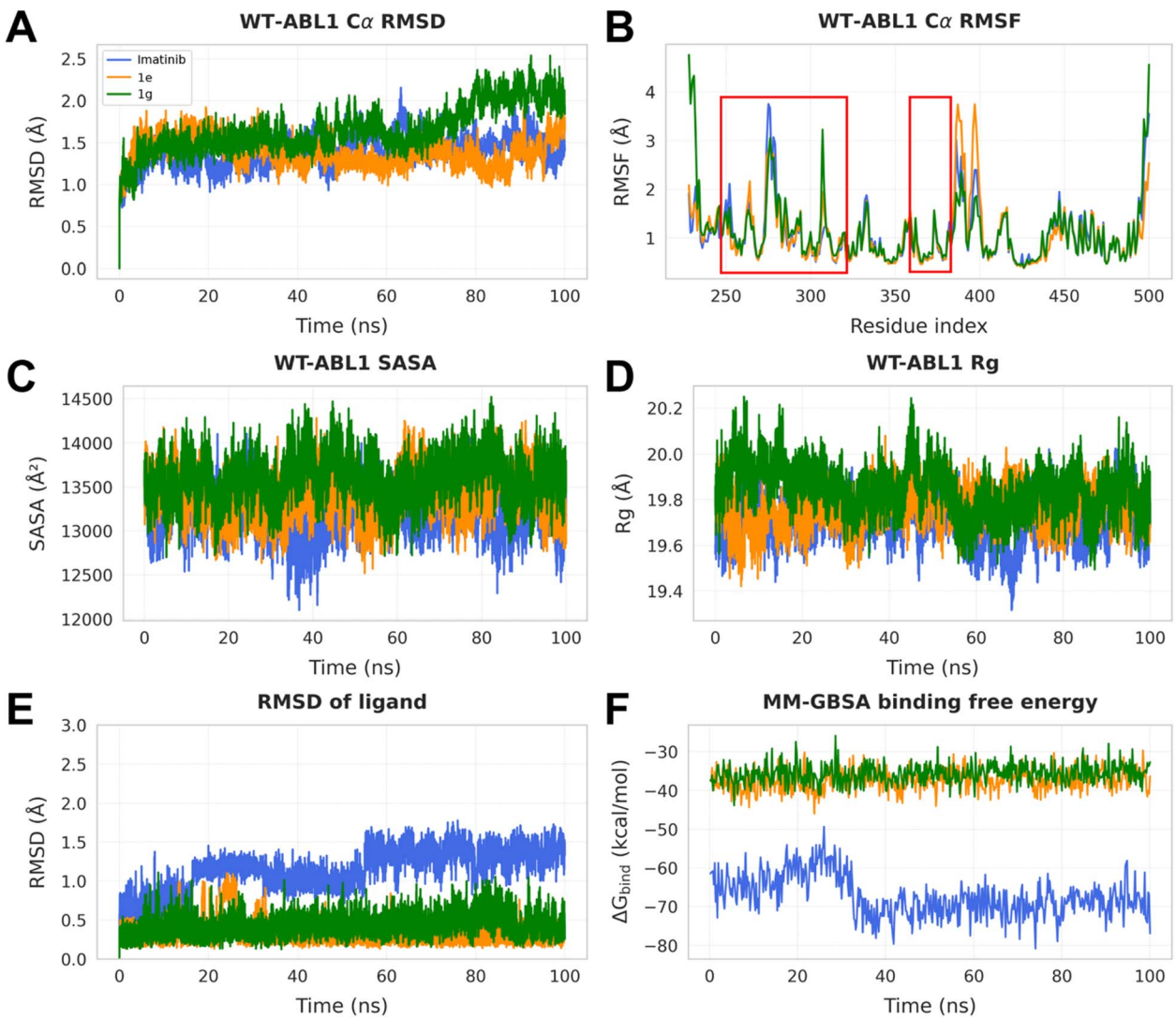

Fig. 3 Analysis of MD simulation trajectories of ABL1 with imatinib (blue), **1e** (orange), and **1g** (green). (A) RMSD of the alpha carbon atoms of wild-type ABL1, (B) RMSF of ABL1 residues, with the red boxes indicating residues within the active site, (C) SASA, (D) radius of gyration of the enzyme, (E) RMSD of the heavy atoms of the ligands, (F) MM-GBSA binding free energy of the ligands to ABL1.

illustrated in Fig. S103.† Table 5 highlights the critical interactions of the ABL1–imatinib complex, which include hydrogen bonds with Glu286, Thr135, Met318, Ile360, and Asp381, as well as π–π interactions with Tyr253, Phe317, and Phe382. Similarly, most of our compounds exhibited π–π or hydrophobic interactions with Tyr253, Phe317, and Phe382, akin to imatinib. However, hydrogen bonding with Glu286 is crucial for the specific interactions that significantly contribute to the ligand–protein affinity and directly influence the inhibitory activity. Experimental studies have demonstrated that Glu286 is a conserved residue (in both wild-type and mutant variants) and forms an ion pair with Lys271 in the N-lobe of ABL1 to stabilize the phosphate group of ATP during phosphorylation. Consequently, many anti-ABL1 drugs, for both wild-type and mutant forms, form hydrogen bonds with Glu286. Notably, compound **1e**, with an –OH substituent at 2′-position, was the only compound to form a hydrogen bond with Glu286 (with a distance of 1.74 Å), comparable to imatinib (2.32 Å) (Fig. S104†). Conversely, the orientation of the –OH or $-OCH_3$ groups at 4′-position precluded hydrogen bonding with Glu286. In future studies, we aim to leverage these insights into structure–activity relationships (SARs) to design novel 2-amino-4,6-diarylpyrimidines capable of forming hydrogen bonds with Glu286 and other key residues such as Thr135, Met318, Ile360, and Asp381. According to the experimental and docking results, both compounds **1e** and **1g** that confirmed their ABL1 inhibitory activity in the above enzyme assay, were chosen for further analysis of binding stability to ABL1 through MD simulations and BFE calculations.

Molecular dynamics simulations and binding free energy calculations. Fig. 3A illustrates the RMSD values of the carbon alpha atoms of ABL1 in complexes with the ligands along the 100 ns MD simulation trajectories. The complex rapidly reached equilibrium after approximately 10 ns of simulations. However, the enzyme complexes with **1e** and imatinib demonstrated greater stability compared with **1g** by the end of the simulation. Similarly, the SASA and radius of gyration (R_g) of the protein remained stable throughout the simulation (Fig. 3C and D). The stability of the three complexes allowed further analyses to evaluate the interactions between the investigated ligands and the enzyme.

The RMSF plot in Fig. 3B reflects the average fluctuations of the ABL1 residues. Here, the residues at the enzyme's active site are considered (Leu248–Met318 and Ile360–Phe382). Overall, most of the residues in the binding site of ABL1 in complexes with the three ligands exhibit similar fluctuations with amplitudes less than 2 Å, except for the Lys274–Glu279 loop (Fig. S105†). Interestingly, the presence of our synthetic compounds caused a decrease in the fluctuations of the residues in this loop compared with imatinib. However, the binding of **1g** resulted in increased fluctuations of Arg307 within the Arg307–Phe311 loop.

Fig. 3E illustrates the ligands' fluctuations, as reflected by the RMSD values of the heavy atoms of the compounds. Both **1e** and **1g** exhibit motion amplitudes less than 1 Å, indicating high stability and the ability to maintain a consistent binding mode with ABL1 throughout the simulation (Fig. S106†). Imatinib shows a change in RMSD starting around 53 ns but eventually stabilizes toward the end of the trajectory. The stability of the ligands is further correlated with the binding free energy in Fig. 3F. Once imatinib reaches equilibrium, the $\Delta G_{\text{MM-GBSA}}$ also becomes stable. Although **1e** and **1g** display higher BFE than imatinib does (-37.33 ± 2.77 and -35.72 ± 2.56 *vs.* -67.31 ± 5.25 kcal mol^{-1}), their binding remains highly stable over the MD simulation time. The calculated BFE values were consistent with the experimental inhibitory activity of the compounds, as **1e** exhibited a lower IC_{50} than **1g** but a higher IC_{50} than imatinib.

The interaction fingerprints of **1e** and **1g** with ABL1 were analyzed using the MDAnalysis and ProLIF programs, resulting in the 2D diagrams shown in Fig. 4. Notably, the amino groups of the 2-amino-4,6-diarylpyrimidine derivatives play a crucial role in forming hydrogen bonds with residues in the enzyme's active site. Specifically, **1e** forms hydrogen bonds with Ala269 and Ile313 with occupancies of 72% and 38%, respectively, while **1g** maintains hydrogen bonding with Thr315 and Glu316

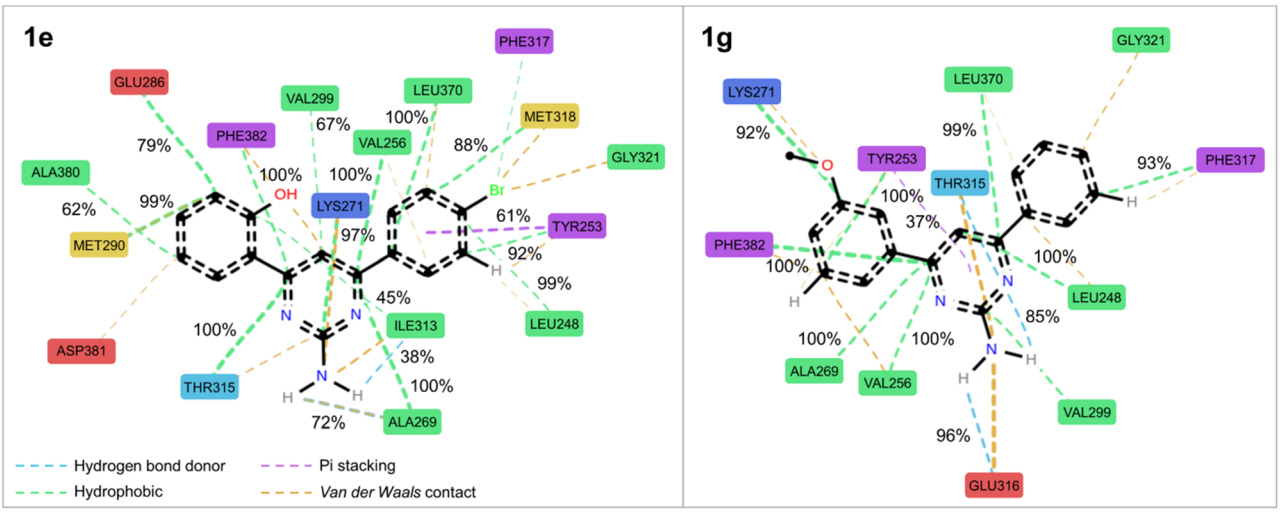

Fig. 4 Occupancy of interactions between **1e** and **1g** with ABL1 along the 100 ns MD simulation trajectories.

Table 6 Comparison of Vina docking scores and binding free energies of ligands with mutant and wild-type ABL1

Ligand	$\Delta G_{\text{vina ABL-1 mutant}}$ (kcal mol^{-1})	$\Delta\Delta G_{\text{dock}}$ (kcal mol^{-1})	$\text{BFE}_{\text{ABL-1 mutant}}$ ($\Delta G_{\text{bind MM-GBSA}}$, kcal mol^{-1})	$\Delta\Delta G_{\text{bind MM-GBSA}}$ (kcal mol^{-1})
PH2HBR	−8.6	0	−36.49	0.84
PH3MA	−9.5	−0.9	−36.08	−0.36
Imatinib	−12.4	1.1	−58.15	9.16

at occupancies of 85% and 96%. The phenyl groups of both compounds participate in π-stacking interactions with Tyr253, Phe317, and Phe382. Additionally, the ligands interact with several other hydrophobic residues within the binding site, such as Leu248, Val256, Lys271, Met290, Val299, Leu370, and Ala380. van der Waals interactions also significantly affect the ligand's binding affinity to the enzyme and are detailed in Table S5.†

The results indicate that **1e** and **1g** are promising and stable inhibitors of wild-type ABL1. The IC_{50} and BFE values highlight the potential of these compounds and suggest that they could be further structurally developed to achieve stronger binding affinity and inhibitory activity.

Prediction of the binding affinity of 1e and 1g on mutant ABL1. **1e** and **1g**, along with imatinib, were docked onto the ABL1 T334I mutant structure (PDB ID 5MO4) to assess their inhibitory potential against drug-resistant CML. The results in Table 6 show that imatinib exhibited a reduced binding affinity to the mutant enzyme ($\Delta\Delta G_{\text{dock}} > 0$). In contrast, the docking score of **1e** remained unchanged ($\Delta\Delta G_{\text{dock}} = 0$). Notably, **1g** showed an increased binding affinity to the ABL1 T334I mutant, with a ΔG_{vina} of −9.5 kcal mol^{-1} (compared with −8.6 kcal-mol^{-1} for the wild-type form). Each complex of ligand and mutant enzyme was subjected to 100 ns MD simulations, similar to the wild-type case. BFE was determined by the use of the MM-GBSA model, and the results were consistent with the docking studies. Imatinib demonstrated a significant reduction in binding affinity to the mutant enzyme ($\Delta\Delta G_{\text{bind MM-GBSA}} > 0$), while the differences in affinity between **1e** and **1g** were negligible. These predictions suggest that both compounds may have potential as inhibitors of the mutant ABL1. However, experimental validation is necessary to confirm these findings.

3. Conclusions

In summary, 17 2-amino-4,6-diarylpyrimidine derivatives with various substituted groups at the 4- and 6-positions, including 1 novel compound **1h**, were synthesized using a two-step approach, which provided several advantages such as time-saving and a simple and mild protocol. Aldol condensation (step 1) of benzaldehydes and acetophenones to produce intermediate chalcones and ring closure condensation (step 2) of chalcones and GHCl were carried out under microwave irradiation to obtain the desired 2-amino-4,6-diarylpyrimidines, with moderate yields and structure characterization by FTIR, 1D- and 2D-NMR, and HRMS analysis. The antiproliferative effect of the synthesized derivatives was then assessed *in vitro* against the CML K562 cell line using the MTT assay, and the active compounds were tested for ABL1 tyrosine kinase inhibition. Compound **1e** had considerable cytotoxic activity against K562 cancer cells and ABL1 tyrosine kinase, with IC_{50} values of 8.77 ± 0.55 μM and 3.35 ± 0.58 μM, respectively. The molecular docking experiment and MD simulations demonstrated that compounds **1e** and **1g** are promising and stable inhibitors of wild-type ABL1 as well as potential inhibitors of the mutant ABL1 (Table 6).

4. Experimental

4.1. Materials and measurements

All the reaction reagents were purchased from Thermo Scientific Chemicals (Belgium). The solvent employed in the procedure required no further purification and was supplied from Chemsol (Vietnam). Merck silica gel 60 F254 plates were used for thin-layer chromatography (TLC). A CEM Discover 2.0 microwave synthesizer was employed in the reaction process. A Bruker Tensor 27 FTIR spectrometer (USA) was used to record Fourier-transform infrared (FTIR) data, with absorption bands measured in wave number (cm^{-1}). A Bruker Advance Neo spectrometer was applied to record ^{1}H (600 MHz) and ^{13}C (125 MHz or 150 MHz) nuclear magnetic resonance (NMR) data, with dimethyl sulfoxide (DMSO) as the solvent. Chemical shifts (δ) were expressed in ppm, coupling constants (J) in hertz, and signal multiplicities were presented as s (singlet), d (doublet), t (triplet), dd (doublet of doublets), dt (doublet of triplets), and m (multiplet). Electrospray ionization (ESI)-high-resolution mass spectrometry (HRMS) data were recorded using ESI-quadrupole time-of-flight (QTOF)-mass spectrometry on a Sciex X500R QTOF system (USA).

4.2. General procedure for the synthesis of 2-amino-4,6-diarylpyrimidine derivatives

Heterocyclic 2-amino-4,6-diarylpyrimidines were synthesized following two steps, as illustrated in Scheme 1. Initially, 17 intermediate chalcones were produced by the aldol condensation of benzaldehydes and acetophenones. The pure chalcones were then ring-closed with GHCl to generate desired derivatives.

In the first step, a mixture of benzaldehydes (3 mmol), acetophenones (3 mmol), and potassium hydroxide (6 mmol) was added to a vessel along with 4 mL of EG. The reaction was conducted for 10 to 30 minutes under MW (100 W, 80 °C) and monitored using TLC to verify the process completion. The reaction mixture was then placed in cold water and neutralized

to pH 7 by HCl, followed by overnight refrigeration. After that, the precipitate was removed by filtering, carefully washing with water, drying, and recrystallizing it from methanol to produce pure intermediates.

In the second step, a mixture of chalcone (1 mmol), GHCl (2 mmol), sodium hydroxide (2 M), and 2 mL of pyridine was introduced into a 25 mL vessel. The reaction was irradiated for 5 to 10 minutes under MW (180 W, 100 °C) and monitored by TLC. Following reaction completion, the mixture was added to ice-cooled water and evaporated in a hood fume. The crude product was then filtered, washed several times with water, vacuum-dried, and recrystallized from methanol, yielding the pure products **1a–1q.**

2-(2-Amino-6-phenylpyrimidin-4-yl)phenol (1a). Pale yellow powder; yield: 41%; R_f = 0.6 (hexane/ethyl acetate, 7 : 3 v/v); FTIR (KBr, ν (cm^{-1})): 3499, 3446 (NH_2), 3345 (OH), 1632 (C=N), 1543 (C=C), 1247 (C–N); ^{1}H-NMR (600 MHz, DMSO-d_6, δ (ppm)): 6.94 (m, 2H, H-3′, H-5′), 7.22 (s, 2H, NH_2), 7.39 (dt, 1H, J = 1.2 Hz, J = 8.4 Hz, H-4′), 7.54 (m, 3H, H-3″, H-4″, H-5″), 7.82 (s, 1H, H-5), 8.25 (m, 3H, H-6′, H-2″, H-6″), 13.99 (s, 1H, OH); ^{13}C-NMR (125 MHz, DMSO-d_6, δ (ppm)): 99.89 (C-5), 117.51 (C-1′), 118.02 (C-3′), 118.62 (C-5′), 127.12 (C-2″, C-6″), 128.02 (C-4″), 128.59 (C-3″, C-5″), 130.73 (C-6′), 132.60 (C-4′), 136.99 (C-1″), 160.30 (C-2′), 161.29 (C-2), 165.19 (C-6), 165.33 (C-4); ESI-HRMS (MeOH): m/z = 264.1134, 264.1137 calcd $[M + H]^+$ for $C_{16}H_{14}N_3O$.

2,2′–(2-Aminopyrimidine-4,6-diyl)diphenol (1b). Pale yellow powder; yield: 51%; R_f = 0.5 (dichloromethane/acetone, 9 : 1 v/v); FTIR (KBr, ν (cm^{-1})): 3449, 3342 (NH_2), 3219 (OH), 1646 (C=N), 1548 (C=C), 1234 (C–N); ^{1}H-NMR (600 MHz, DMSO-d_6, δ (ppm)): 6.96 (m, 4H, H-3′, H-5′, H-3″, H-5″), 7.41 (dt, 2H, J = 1.8 Hz, J = 8.4 Hz, H-4′, H-4″), 7.63 (s, 2H, NH_2), 7.91 (s, 1H, H-5), 8.29 (dd, 2H, J = 1.2 Hz, J = 8.4 Hz, H-6′, H-6″), 13.75 (s, 2H, OH); ^{13}C-NMR (150 MHz, DMSO-d_6, δ (ppm)): 98.26 (C-5), 117.39 (C-1′, C-1″), 118.12 (C-3′, C-3″), 118.71 (C-5′, C-5″), 128.36 (C-6′, C-6″), 132.95 (C-4′, C-4″), 158.94 (C-2), 160.32 (C-2′, C-2″), 165.62 (C-4, C-6); ESI-HRMS (MeOH): m/z = 280.1091, 280.1086 calcd $[M + H]^+$ for $C_{16}H_{14}N_3O_2$.

2-(2-Amino-6-(3-methoxyphenyl)pyrimidin-4-yl)phenol (1c). Pale yellow powder; yield: 56%; R_f = 0.6 (hexane/ethyl acetate, 7 : 3 v/v); FTIR (KBr, ν (cm^{-1})): 3458, 3341 (NH_2), 3227 (OH), 1636 (C=N), 1545 (C=C), 1243 (C–N), 1043 (OCH_3); ^{1}H-NMR (600 MHz, DMSO-d_6, δ (ppm)): 3.87 (s, 3H, OCH_3), 6.95 (m, 2H, H-3′, H-5′), 7.12 (dd, 1H, J = 2.4, J = 8.4 Hz, H-4″), 7.21 (s, 2H, NH_2), 7.39 (dt, 1H, J = 1.2 Hz, J = 8.4 Hz, H-4′), 7.46 (t, 1H, J = 8.4 Hz, H-5″), 7.78 (s, 1H, H-2″), 7.81 (s, 1H, H-5), 7.84 (d, 1H, J = 7.8 Hz, H-6″), 8.26 (d, 1H, J = 8.4 Hz, H-6′), 13.98 (s, 1H, OH); ^{13}C-NMR (150 MHz, DMSO-d_6, δ (ppm)): 55.26 (OCH_3), 100.06 (C-5), 112.29 (C-2″), 116.44 (C-4″), 117.49 (C-1′), 117.99 (C-3′), 118.56 (C-5′), 119.53 (C-6″), 128.08 (C-6′), 129.63 (C-5″), 132.57 (C-4′), 138.50 (C-1″), 159.56 (C-3″), 160.29 (C-2′), 161.22 (C-2), 165.11 (C-6), 165.19 (C-4); ESI-HRMS (MeOH): m/z = 294.1247, 294.1243 calcd $[M + H]^+$ for $C_{17}H_{16}N_3O_2$.

2-(2-Amino-6-(4-methoxyphenyl)pyrimidin-4-yl)phenol (1d). Pale yellow powder; yield: 43%; R_f = 0.4 (hexane/ethyl acetate, 7 : 3 v/v); FTIR (KBr, ν (cm^{-1})): 3464, 3344 (NH_2), 3219 (OH), 1579 (C=N), 1538 (C=C), 1250 (C–N), 1031 (OCH_3); ^{1}H-NMR (600 MHz, DMSO-d_6, δ (ppm)): 3.85 (s, 3H, OCH_3), 6.94 (m, 2H, H-3′, H-5′), 7.09 (m, 2H, H-3″, H-5″), 7.12 (s, 2H, NH_2), 7.38 (dt, 1H, J = 1.8 Hz, J = 8.4 Hz, H-4′), 7.77 (s, 1H, H-5), 8.25 (m, 3H, H-6′, H-2″, H-6″), 14.08 (s, 1H, OH); ^{13}C-NMR (125 MHz, DMSO-d_6, δ (ppm)): 55.31 (OCH_3), 98.99 (C-5), 113.93 (C-3″, C-5″), 117.57 (C-1′), 117.98 (C-3′), 118.52 (C-5′), 127.90 (C-6′), 128.76 (C-2″, C-6″), 129.23 (C-1″), 132.43 (C-4′), 160.30 (C-2′), 161.14 (C-6), 161.49 (C-2, C-4″), 164.86 (C-4); ESI-HRMS (MeOH): m/z = 294.1248, 294.1243 calcd $[M + H]^+$ for $C_{17}H_{16}N_3O_2$.

2-(2-Amino-6-(4-bromophenyl)pyrimidin-4-yl)phenol (1e). Pale yellow powder; yield: 33%; R_f = 0.6 (chloroform/methanol, 9 : 1 v/v); FTIR (KBr, ν (cm^{-1})): 3498, 3348 (NH_2), 3215 (OH), 1638 (C=N), 1545 (C=C), 1253 (C–N), 579 (C–Br); ^{1}H-NMR (600 MHz, DMSO-d_6, δ (ppm)): 6.95 (m, 2H, H-3′, H-5′), 7.25 (s, 2H, NH_2), 7.39 (dt, 1H, J = 1.2 Hz, J = 8.4 Hz, H-4′), 7.75 (d, 2H, J = 8.4 Hz, H-3″, H-5″), 7.85 (s, 1H, H-5), 8.24 (m, 3H, H-6′, H-2″, H-6″), 13.92 (s, 1H, OH); ^{13}C-NMR (125 MHz, DMSO-d_6, δ (ppm)): 98.80 (C-5), 117.43 (C-1′), 118.02 (C-3′), 118.59 (C-5′), 124.42 (C-4″), 128.07 (C-6′), 129.13 (C-2″, C-6″), 131.56 (C-3″, C-5″), 132.67 (C-4′), 136.14 (C-1″), 160.29 (C-2′), 161.26 (C-2), 164.06 (C-6), 165.45 (C-4); ESI-HRMS (MeOH): m/z = 342.0239, 342.0242 calcd $[M + H]^+$ for $C_{16}H_{13}BrN_3O$.

2-(2-Amino-6-(4-chlorophenyl)pyrimidin-4-yl)phenol (1f). Pale yellow powder; yield: 31%; R_f = 0.6 (hexane/ethyl acetate, 7 : 3 v/v); FTIR (KBr, ν (cm^{-1})): 3503 (OH), 3345, 3215 (NH_2), 1640 (C=N), 1547 (C=C), 1264 (C–N), 747 (C–Cl); ^{1}H-NMR (600 MHz, DMSO-d_6, δ (ppm)): 6.95 (m, 2H, H-3′, H-5′), 7.24 (s, 2H, NH_2), 7.39 (t, 1H, J = 7.8 Hz, H-4′), 7.61 (d, 2H, J = 8.4 Hz, H-3″, H-5″), 7.85 (s, 1H, H-5), 8.24 (d, 1H, J = 7.8 Hz, H-6′), 8.29 (d, 2H, J = 8.4 Hz, H-2″, H-6″), 13.93 (s, 1H, OH); ^{13}C-NMR (125 MHz, DMSO-d_6, δ (ppm)): 99.83 (C-5), 117.43 (C-1′), 118.01 (C-3′), 118.58 (C-5′), 128.07 (C-6′), 128.62 (C-3″, C-5″), 128.90 (C-2″, C-6″), 132.66 (C-4′), 135.52 (C-1″), 135.78 (C-4″), 160.29 (C-2′), 161.25 (C-2), 163.96 (C-6), 165.43 (C-4); ESI-HRMS (MeOH): m/z = 298.0753, 298.0747 calcd $[M + H]^+$ for $C_{16}H_{13}ClN_3O$.

4-(3-Methoxy-phenyl)-6-phenyl-pyrimidin-2-ylamine (1g). Pale yellow powder; yield: 36%; R_f = 0.47 (hexane/ethyl acetate, 7 : 3 v/v); FTIR (KBr, ν (cm^{-1})): 3450, 3429 (NH_2), 1632 (C=N), 1566 (C=C), 1260 (C–N), 1038 (OCH_3); ^{1}H-NMR (600 MHz, DMSO-d_6, δ (ppm)): 3.85 (s, 3H, OCH_3), 6.73 (s, 2H, NH_2), 7.09 (dd, 1H, J = 2.4 Hz, J = 7.8 Hz, H-4′), 7.44 (t, 1H, J = 7.8 Hz, H-5′), 7.52 (m, 3H, H-3″, H-4″, H-5″); 7.69 (s, 1H, H-5), 7.76 (s, 1H, H-2′), 7.80 (d, 1H, J = 7.8 Hz, H-6′), 8.23 (m, 2H, H-2″, H-6″); ^{13}C-NMR (125 MHz, DMSO-d_6, δ (ppm)): 55.25 (OCH_3), 102.02 (C-5), 112.13 (C-2′), 116.13 (C-4′), 119.36 (C-6′), 126.96 (C-2″, C-6″), 128.54 (C-3″, C-5″), 129.63 (C-5′), 130.38 (C-4″), 137.30 (C-1″), 138.86 (C-1′), 159.57 (C-3′), 163.92 (C-2), 164.67 (C-6), 164.88 (C-4); ESI-HRMS (MeOH): m/z = 278.1298, 278.1293 calcd $[M + H]^+$ for $C_{17}H_{16}N_3O$.

4-(2-Amino-6-(3-methoxy-phenyl)-pyrimidin-4-yl)-phenol (1h). Pale brown powder; yield: 48%; R_f = 0.63 (hexane/ethyl acetate, 4 : 6 v/v); FTIR (KBr, ν (cm^{-1})): 3517 (OH), 3403 (NH), 1608 (C=N), 1542 (C=C), 1241 (C–N), 1037 (OCH_3); ^{1}H-NMR (600 MHz, DMSO-d_6, δ (ppm)): 3.85 (s, 3H, OCH_3), 6.58 (2H, s, NH_2), 6.87 (d, 2H, J = 9.0 Hz, H-3″, H-5″), 7.07 (dd, 1H, J = 2.4 Hz, J = 7.8 Hz, H-4′), 7.42 (t, 1H, J = 7.8 Hz, H-5′), 7.57 (s, 1H, H-5), 7.72 (s, 1H, H-2′), 7.77 (d, 1H, J = 7.8 Hz, H-6′), 8.09 (d, 2H, J =

9.0 Hz, H-2″, H-6″), 9.89 (s, 1H, OH); ^{13}C-NMR (125 MHz, DMSO-d_6, δ (ppm)): 55.22 (OCH_3), 100.93 (C-5), 112.00 (C-2′), 115.25 (C-3″, C-5″), 115.95 (C-4′), 119.26 (C-6′), 127.99 (C-1″), 128.63 (C-2″, C-6″), 129.56 (C-5′), 139.08 (C-1′), 159.53 (C-3′), 159.74 (C-4″), 163.78 (C-2), 164.12 (C-4), 164.68 (C-6); ESI-HRMS (MeOH): m/z = 294.1249, 294.1242 calcd $[M + H]^+$ for $C_{17}H_{16}N_3O_2$.

4-(4-Methoxy-phenyl)-6-(3-methoxy-phenyl)-pyrimidin-2-ylamine (1i). Pale yellow powder; yield: 45%; R_f = 0.43 (hexane/ethyl acetate, 4 : 2 v/v); FTIR (KBr, ν (cm^{-1})): 3428, 3310 (NH_2), 1641 (C=N), 1566 (C=C), 1245 (C–N), 1032 (OCH_3); ^{1}H-NMR (600 MHz, DMSO-d_6, δ (ppm)): 3.84 (s, 3H, OCH_3), 3.85 (s, 3H, OCH_3), 6.64 (s, 2H, NH_2), 7.09 (m, 3H, H-4′, H-3″, H-5″), 7.44 (t, 1H, J = 7.8 Hz, H-5′), 7.64 (s, 1H, H-5), 7.75 (s, 1H, H-2), 7,79 (d, 1H, J = 7.8 Hz, H-6′), 8,21 (d, 2H, J = 7.2 Hz, H-2″, H-6″); ^{13}C-NMR (150 MHz, DMSO-d_6, δ (ppm)): 55.21 (OCH_3), 55.25 (OCH_3), 101.21 (C-5), 112.09 (C-2′), 113.86 (C-3″, C-5″), 115.95 (C-4′), 119.28 (C-6′), 128.52 (C-2″, C-6″), 129.55 (C-5′), 129.57 (C-1″), 138.99 (C-1′), 159.52 (C-3′), 161.19 (C-4″), 163.80 (C-2), 164.31 (C-4), 164.39 (C-6); ESI-HRMS (MeOH): m/z = 308.1400, 308.1399 calcd $[M + H]^+$ for $C_{18}H_{18}N_3O$.

4-(4-Bromo-phenyl)-6-(3-methoxy-phenyl)-pyrimidin-2-ylamine (1j). Pale yellow powder; yield: 55%; R_f = 0.61 (hexane/acetone, 4 : 2 v/v); FTIR (KBr, ν (cm^{-1})): 3459, 3318 (–NH_2), 1638 (C=N), 1542 (C=C), 1260 (C–N), 1034 (OCH_3), 593 (C–Br); ^{1}H-NMR (600 MHz, DMSO-d_6, δ (ppm)): 3.86 (s, 3H, OCH_3), 6.77 (s, 2H, NH_2), 7.10 (dd, J = 2.4 Hz, J = 6.0 Hz, 1H, H-4′), 7.45 (t, 1H, J = 7.8 Hz, H-5′), 7.73 (m, 3H, H-5, H-3″, H-5″), 7.76 (s, 1H, H-2), 7.81 (d, 1H, J = 7.8 Hz, H-6′), 8.20 (d, 2H, J = 7.2 Hz, H-2″, H-6″); ^{13}C-NMR (125 MHz, DMSO-d_6, δ (ppm)): 55.32 (OCH_3), 101.94 (C-5), 112.22 (C-2′), 116.29 (C-4′), 119.45 (C-6′), 124.11 (C-4″), 129.08 (C-2″, C-6″), 129.73 (C-5′), 131.61 (C-3″, C-5″), 136.51 (C-1″), 138.75 (C-1′), 159.63 (C-3′), 163.73 (C-6), 163.95 (C-2), 164.99 (C-4); ESI-HRMS (MeOH): m/z = 356.0397, 356.0398 calcd $[M + H]^+$ for $C_{17}H_{15}BrN_3O$.

4-(4-Chloro-phenyl)-6-(3-methoxy-phenyl)-pyrimidin-2-ylamine (1k). Pale yellow powder; yield: 48%; R_f = 0.38 (hexane/diethyl ether, 5 : 5 v/v); FTIR (KBr, ν (cm^{-1})): 3319, 3204 (NH_2), 1639 (C=N), 1544 (C=C), 1261 (C–N), 1035 (OCH_3), 784 (C–Cl); ^{1}H-NMR (600 MHz, DMSO-d_6, δ (ppm)): 3.85 (s, 3H, OCH_3), 6.76 (s, 2H, NH_2), 7.09 (dd, J = 2.4 Hz, J = 7.8 Hz, 1H, H-4′), 7.44 (t, 1H, J = 7.8 Hz, H-5′), 7.59 (d, 2H, J = 6.6 Hz, H-3″, H-5″), 7.72 (s, 1H, H-5), 7.76 (s, 1H, H-2′), 7.80 (d, 1H, J = 7.8 Hz, H-6′), 8.26 (d, 2H, J = 6.6 Hz, H-2″, H-6″); ^{13}C-NMR (150 MHz, DMSO-d_6, δ (ppm)): 55.26 (OCH_3), 101.91 (C-5), 112.19 (C-2′), 116.21 (C-4′), 119.40 (C-6′), 128.60 (C-3″, C-5″), 128.77 (C-2″, C-6″), 129.65 (C-5′), 135.19 (C-4″), 136.11 (C-1″), 138.73 (C-1′), 159.58 (C-3′), 163.57 (C-6), 163.90 (C-2), 164.90 (C-4); ESI-HRMS (MeOH): m/z = 312.0902, 312.0904 calcd $[M + H]^+$ for $C_{17}H_{15}ClN_3O$.

4-(4-Methoxyphenyl)-6-phenylpyrimidin-2-amine (1l). Pale yellow orange powder; yield: 47%; R_f = 0.46 (hexane/ethyl acetate, 4 : 2 v/v); FTIR (KBr, ν (cm^{-1})): 3364, 3326 (NH_2), 1644 (C=N), 1587 (C=C), 1258 (C–N), 1031 (OCH_3); ^{1}H-NMR (600 MHz, DMSO-d_6, δ (ppm)): 3.84 (s, 3H, OCH_3), 6.64 (s, 2H, NH_2), 7.08 (d, 2H, J = 9.0 Hz, H-3′, H-5′), 7.54 (m, 3H, H-3″, H-4″, H-5″), 7.65 (s, 1H, H-5), 8.22 (m, 4H, H-2′, H-6′, H-2″, H-6″); ^{13}C-NMR (150 MHz, DMSO-d_6, δ (ppm)): 55.30 (OCH_3), 101.07 (C-5), 113.93 (C-3′, C-5′), 126.90 (C-2′, C-6′), 128.53 (C-2″, C-6″), 128.54 (C-3″, C-5″), 129.62 (C-1′), 130.28 (C-4″), 137.48 (C-1″), 161.23 (C-4′), 163.90 (C-2), 164.42 (C-6), 164.56 (C-4); ESI-HRMS (MeOH): m/z = 278.1298, 278.1293 calcd $[M + H]^+$ for $C_{17}H_{16}N_3O$.

4-(2-Amino-6-(4-methoxyphenyl)pyrimidin-4-yl)phenol (1m). Pale yellow brown powder; yield: 42%; R_f = 0.47 (hexane/acetone, 4 : 2 v/v); FTIR (KBr, ν (cm^{-1})): 3504 (OH), 3387 (NH), 1568 (C=N), 1537 (C=C), 1233 (C–N), 1176 (OCH_3); ^{1}H-NMR (600 MHz, DMSO-d_6, δ (ppm)): 3.83 (s, 3H, OCH_3), 6.49 (s, 2H, NH_2), 6.88 (d, 2H, J = 6.6 Hz, H-3″, H-5″), 7.05 (d, 2H, J = 6.6 Hz, H-3′, H-5′), 7.53 (s, 1H, H-5), 8.08 (d, 2H, J = 6.6 Hz, H-2″, H-6″), 8.17 (d, 2H, J = 6.6 Hz, H-2′, H-6′), 9.90 (s, 1H, OH); ^{13}C-NMR (150 MHz, DMSO-d_6, δ (ppm)): 55.25 (OCH_3), 99.97 (C-5), 113.84 (C-3′, C-5′), 115.24 (C-3″, C-5″), 128.15 (C-1″), 128.38 (C-2′, C-6′), 128.51 (C-2″, C-6″), 129.82 (C-1′), 159.64 (C-4″), 161.05 (C-4′), 163.74 (C-4), 163.89 (C-6), 164.38 (C-2); ESI-HRMS (MeOH): m/z = 294.1244, 294.1243 calcd $[M + H]^+$ for $C_{17}H_{16}N_3O_2$.

4,6-Bis(4-methoxyphenyl)pyrimidin-2-amine (1n). Pale yellow powder; yield: 33%; R_f = 0.31 (hexane/ethyl acetate, 4 : 2 v/v); FTIR (KBr, ν (cm^{-1})): 3331, 3202 (NH_2), 1648 (C=N), 1584 (C=C), 1236 (C–N), 1028 (OCH_3); ^{1}H-NMR (600 MHz, DMSO-d_6, δ (ppm)): 3.84 (s, 6H, OCH_3), 6.55 (s, 2H, NH_2), 7.07 (d, 4H, J = 9.0 Hz, H-3′, H-5′, H-3″, H-5″), 7.59 (s, 1H, H-5), 8.20 (d, 4H, J = 9.0 Hz, H-2′, H-6′, H-2″, H-6″); ^{13}C-NMR (150 MHz, DMSO-d_6, δ (ppm)): 55.25 (OCH_3), 100.24 (C-5), 113.84 (C-3′, C-5′, C-3″, C-5″), 128.43 (C-2′, C-6′, C-2″, C-6″), 129.74 (C-1′, C-1″), 161.09 (C-4′, C-4″), 163.77 (C-2), 164.07 (C-4, C-6); ESI-HRMS (MeOH): m/z = 308.1400, 308.1399 calcd $[M + H]^+$ for $C_{18}H_{18}N_3O_2$.

4-(4-Bromophenyl)-6-(4-methoxyphenyl)pyrimidin-2-amine (1o). Pale yellow powder; yield: 48%; R_f = 0.32 (hexane/acetone, 4 : 2 v/v); FTIR (KBr, ν (cm^{-1})): 3367, 3212 (NH_2), 1645 (C=N), 1588 (C=C), 1255 (C–N), 1033 (OCH_3), 592 (C–Br); ^{1}H-NMR (600 MHz, DMSO-d_6, δ (ppm)): 3.89 (s, 3H, OCH_3), 6.73 (s, 2H, NH_2), 7.12 (d, 2H, J = 9.0 Hz, H-3′, H-5′), 7.73 (s, 1H, H-5), 7.77 (d, 2H, J = 9.0 Hz, H-3″, H-5″), 8.23 (d, 2H, J = 8.4 Hz, H-2″, H-6″), 8.26 (d, 2H, J = 9.0 Hz, H-2′, H-6′); ^{13}C-NMR (150 MHz, DMSO-d_6, δ (ppm)): 55.29 (OCH_3), 100.09 (C-5), 113.91 (C-3′, C-5′), 123.89 (C-4″), 128.56 (C-2′, C-6′), 128.93 (C-2″, C-6″), 129.47 (C-1′), 131.51 (C-3″, C-5″), 136.64 (C-1″), 161.29 (C-4′), 163.29 (C-6), 163.86 (C-2), 164.65 (C-4); ESI-HRMS (MeOH): m/z = 356.0397, 356.0398 calcd $[M + H]^+$ for $C_{17}H_{15}BrN_3O$.

4-(4-Chlorophenyl)-6-(4-methoxyphenyl)pyrimidin-2-amine (1p). Pale yellow powder; yield: 64%; R_f = 0.54 (hexane/ethyl acetate, 4 : 2 v/v); FTIR (KBr, ν (cm^{-1})): 3331, 3210 (NH_2), 1644 (C=N), 1562 (C=C), 1238 (C–N), 1032 (OCH_3), 815 (C–Cl); ^{1}H-NMR (600 MHz, DMSO-d_6, δ (ppm)): 3.84 (s, 3H, OCH_3), 6.68 (s, 2H, NH_2), 7.07 (d, 2H, J = 9.0 Hz, H-3′, H-5′), 7.58 (d, 2H, J = 8.4 Hz, H-3″, H-5″), 7.67 (s, 1H, H-5), 8.21 (d, 2H, J = 9.0 Hz, H-2′, H-6′), 8.25 (d, 2H, J = 8.4 Hz, H-2″, H-6″); ^{13}C-NMR (150 MHz, DMSO-d_6, δ (ppm)): 55.27 (OCH_3), 100.93 (C-5), 113.89 (C-3′, C-5′), 128.55 (C-2″, C-3″, C-5″, C-6″), 128.67 (C-2′, C-6′), 129.47 (C-1′), 135.02 (C-4″), 136.26 (C-1″), 161.27 (C-4′), 163.19 (C-6), 163.84 (C-2), 164.61 (C-4); ESI-HRMS (MeOH): m/z = 312.0908, 312.0904 calcd $[M + H]^+$ for $C_{17}H_{15}ClN_3O$.

4-(2-Amino-6-phenyl-pyrimidin-4-yl)-phenol (1q). Pale brown powder; yield: 44%; R_f = 0.49 (chloroform/methanol, 99 : 1 v/v); FTIR (KBr, ν (cm^{-1})): 3506, 3399 (NH_2), 3057 (OH), 1602 (C=N),

1539 (C=C), 1231 (C–N); ^{1}H-NMR (600 MHz, DMSO-d_6, δ (ppm)): 6.59 (s, 2H, NH_2), 6.89 (d, 2H, J = 8.4 Hz, H-3′, H-5′), 7.51 (m, 3H, H-3″, H-4″, H-5″); 7.59 (s, 1H, H-5), 8.10 (d, 2H, J = 9.0 Hz, H-2′, H-6′), 8.19 (m, 2H, H-2″, H-6″), 9.91 (s, 1H, OH), ^{13}C-NMR (125 MHz, DMSO-d_6, δ (ppm)): 100.78 (C-5), 115.28 (C-3′, C-5′), 126.82 (C-2″, C-6″), 128.03 (C-1′), 128.49 (C-3″, C-5″), 128.58 (C-2′, C-6′), 130.17 (C-4″), 137.54 (C-1″), 159.72 (C-4′), 163.84 (C-2), 164.34 (C-6), 164.69 (C-4); ESI-HRMS (MeOH): m/z = 264.1141, 264.1137 calcd $[M + H]^+$ for $C_{16}H_{14}N_3O$.

4.3. Cytotoxicity assay

Anti-proliferative activity on K562 cell line. The main paragraph text follows directly on here. The human CML K562 cell line was subjected to the MTT (3-(4,5-dimethylthiazol-2-yl)-2,5-diphenyl tetrazolium bromide) test to determine the anticancer activity of all the 2-amino-4,6-diarylpyrimidine compounds **1a–1q**. The investigated compounds were dissolved in DMSO to create a stock solution (100 mM), which was subsequently diluted to produce different concentrations. DMSO and imatinib were used as a blank control and a reference drug, respectively. The cancer cells were cultivated in RPMI 1640 medium supplemented with 10% fetal bovine serum, 1% of penicillin (100 units per mL), and 100 μg mL^{-1} of streptomycin sulfate at 37 °C and 5% CO_2 for 24 hours following Mosmann's protocol.[36] The cells were then plated into 96-well plates at a 200 μL volume and 5×10^4 cells density per well. After 24 hours, the cells were treated with pre-prepared test compounds at varying concentrations. After 48 hours, 20 μL of MTT (5 mg mL^{-1} dissolved in PBS) was applied to the cells and incubated for 3 to 4 hours at 37 °C in 5% CO_2. The culture media were then carefully removed, and isopropanol was used to dissolve the formazan precipitate. The absorbance was measured at the wavelength of 570 nm. Each concentration of tested compounds was investigated in triplicate. As a positive control, imatinib was employed. The following formula was used to calculate the percentage of cell survival (CS):

$$\mathrm{CS}\ (\%) = \left[\frac{\mathrm{OD(test\ sample)}}{\mathrm{OD(control)}} \times 100\right]$$

For the compounds that have CS values less than 50% in the first screening, the IC_{50} values (μM) were determined using nonlinear regression analysis in GraphPad Prism 5.0.

ABL1 tyrosine kinase inhibition in K562 cells. Sandwich enzyme-linked immunosorbent assay (ELISA) is the basis for the human ABL1 ELISA kit (FineTest, Cat: EH4452). Anti-ABL1 antibodies were pre-coated onto a 96-well plate. Biotin-labeled anti-ABL1 antibodies were used for detecting ABL1. Test samples and ABL1 standards at various concentrations were incubated in the wells. After incubation, unbound biotin was removed by washing with buffer. Then, HRP–streptavidin conjugated detection antibodies were added. After the third wash, the TMB substrate was added to initiate the HRP enzymatic reaction. The HRP catalyzed TMB to produce a blue color, which turned yellow after the stop solution was added. An ELISA reader was used to read the 96-well plate at a 450 nm wavelength. The concentration of ABL1 in the samples was calculated on the basis of the ABL1 standard curve. The detailed process is as follows: the well was filled with 100 μL of the standard or test sample, sealed, and incubated at 37 °C for 90 minutes, followed by washing twice without soaking. Then, 100 μL of biotinylated antibody solution was added, incubated at 37 °C for 60 minutes, and washed three times with a 1 minute soak. Next, 100 μL of SABC solution was added, incubated for 30 minutes, and washed five times with a 1 minute soak. Afterward, 90 μL of TMB solution was added, and the mixture was incubated at 37 °C for 10 to 20 minutes. Finally, 50 μL of stop solution was added, and the plate was read at 450 nm wavelength. The concentration of ABL1 was calculated using CurveExpert 1.4 software. The test sample was diluted 20 times.

4.4. Computational analysis

Selection of the 3D structures of ABL1 kinase for computational simulations. The 3D structures of human tyrosine-protein kinase ABL1 (EC 2.7.10.2) were queried from the RCSB Protein Data Bank (PDB)[37] using the UniProt ID P00519. A total of 72 PDB entries, determined by X-ray crystallography, were found. In this study, PDB complexes containing imatinib were of particular interest, as this ABL1 kinase inhibitor was utilized as a positive control in experimental assays. Therefore, the co-crystallized structure of wild-type ABL1 with imatinib (PDB ID 2HYY)[38] was used in molecular docking simulations to assess the binding affinity of 2-amino-4,6-diarylpyrimidine derivatives to the enzyme.

Although imatinib remains the first-line treatment for CML, drug-resistant mutations, most notably ABL1 T334I, have significantly reduced its long-term efficacy.[39] Therefore, the investigated compounds are evaluated for their potential inhibition against drug-resistant CML. We also searched for PDB structures of ABL1 kinase mutants for simulation purposes. However, no crystal structure of the mutant enzyme–imatinib complex exists at the ATP-binding site. As a result, the co-crystallized structure of the ABL1 T334I-D382N mutant with nilotinib (PDB ID 5MO4)[40] was employed for docking studies. In this study, nilotinib was used exclusively to validate the docking model for mutant ABL1. The binding affinity of 2-amino-4,6-diarylpyrimidine derivatives at the active site of the ABL1 T334I mutant was then evaluated using imatinib as the reference.

Molecular docking studies. Polar hydrogens were added to the 3D structure of ABL1 kinase (wild-type or mutant), and Kollman charges were assigned using AutoDock Tools 1.5.7 software.[41] Grid boxes were defined on the basis of the coordinates of imatinib in the PDB 2HYY. AutoDock Vina 1.1.2 was used for molecular docking[42] with the following parameters: exhaustiveness = 16, energy range = 4, number of retained poses = 10, and random seed = 42. Redocking imatinib into PDB 2HYY and nilotinib into PDB 5MO4 confirmed the docking process. Subsequently, the investigated compounds were docked onto both the wild-type and mutant forms of ABL1 kinase, with imatinib serving as the reference ligand. The binding affinities of the compounds were assessed based on

Vina binding energy (ΔG_{vina}) and their interactions with enzyme residues in active site (visualized by the PoseView web tool).[42,43]

Molecular dynamics simulations and binding free energy calculations. The stability of the binding of inhibitors to ABL1 kinase was investigated through molecular dynamics (MD) simulations. Each previously docked protein–ligand complex was subjected to a 100 ns MD simulation using Amber24 software,[44] following a previously published protocol.[45] MD trajectories were analyzed with the *cpptraj* module[46] in AmberTools24.[45] The protein–ligand stability was assessed using RMSD, RMSF, R_g, and solvent-accessible surface area (SASA) plots, which were analyzed on the basis of the carbon alpha of ABL1 kinase. The stability of the inhibitors within the enzyme's active site was assessed using RMSD plots of ligands heavy atoms. Binding free energy (BFE) was computed from the MD simulation trajectories using the *MMPBSA.py* tool[47] in AmberTools24 on the basis of molecular mechanics with the generalized Born surface area (MM-GBSA) model. The BFE was computed according to eqn (1)

$$\Delta G_{bind} = \Delta G_{complex} - (\Delta G_{enzyme} + \Delta G_{inhibitor}) \quad (1)$$

The occupancy of interactions between ligands and enzyme residues during MD simulations was analyzed using interaction fingerprints with the ProLIF and MDAnalysis tools.[48,49]

Data availability

The data supporting this article have been included as part of the ESI,† including the FTIR, HRMS, 1D-, 2D-NMR spectra of synthesized derivatives, the cell survival results of K562 cytotoxic activity, and the computational data of compounds and Imatinib on ABL1 tyrosine kinase.

Author contributions

Thi-Anh-Truc Phan and Kim-Khanh-Huy Ngo: conceptualization, data curation, formal analysis, methodology, validation, visualization, writing – original draft, and writing – review & editing, Thi-Cam-Thu Nguyen: writing – original draft, and writing – review & editing, Thanh-Tan Mai: data curation, formal analysis, methodology, software, validation, visualization, and writing – review & editing, Hai-Dang Nguyen and Thu-Trang Duong: data curation, formal analysis, methodology, validation, visualization, and writing – review & editing, Le-Phu Tran, Thanh-Tuyen Duong, Thi-Kim-Chi Huynh, Elena V. Koroleva, Zhanna V. Ignatovich, Anastasiya L. Ermolinskaya, Hoang-Phuc Nguyen, Thi-Hong-An Nguyen, Anh-Khoa Ton, Tuong-Ha Do: formal analysis, and writing – review & editing, Thi-Kim-Dung Hoang: conceptualization, funding acquisition, methodology, project administration, resources, supervision, validation, and writing – review & editing.

Conflicts of interest

There are no conflicts to declare.

Acknowledgements

This research is funded by the Vietnam Academy of Science and Technology under grant number QTBY01.04/23-24.

References

1 W. Peng, G. A. de Tuya, A. A. Eduardo, J. A. Vishny and Q. Huang, *Publ. Understand. Sci.*, 2022, **31**, 53–69.
2 J. D. Mizrahi, R. Surana, J. W. Valle and R. T. Shroff, *Lancet*, 2020, **395**, 2008–2020.
3 R. L. Siegel, K. D. Miller and A. Jemal, *Ca-Cancer J. Clin.*, 2020, **70**, 7–30.
4 A. S. Davis, A. J. Viera and M. D. Mead, *Am. Fam. Physician*, 2014, **89**, 731–738.
5 D. G. Gilliland, C. T. Jordan and C. A. Felix, *Hematol. Am. Soc. Hematol. Educ. Program*, 2004, **2004**, 80–97.
6 J. V. Melo, T. P. Hughes and J. F. Apperley, *Hematol. Am. Soc. Hematol. Educ. Program*, 2003, **2003**, 132–152.
7 M. W. Deininger, J. M. Goldman and J. V. Melo, *Blood*, 2000, **96**, 3343–3356.
8 A. Quintás-Cardama and J. E. Cortes, *Mayo Clin. Proc.*, 2006, **81**, 973–988.
9 M. Baccarani and R. P. Gale, *Leukemia*, 2021, **35**, 2199–2204.
10 E. Klein, F. Vánky, H. Ben-Bassat, H. Neumann, P. Ralph, J. Zeuthen and A. Polliack, *Int. J. Cancer*, 1976, **18**, 421–431.
11 F. Luchetti, A. Gregorini, S. Papa, S. Burattini, B. Canonico, M. Valentini and E. Falcieri, *Haematologica*, 1998, **83**, 974–980.
12 B. Druker, *N. Engl. J. Med.*, 2001, **345**, 232.
13 M. Okada, S. Adachi, T. Imai, K.-i. Watanabe, S.-y. Toyokuni, M. Ueno, A. S. Zervos, G. Kroemer and T. Nakahata, *Blood*, 2004, **103**, 2299–2307.
14 E. Koroleva, Z. I. Ignatovich, Y. V. Sinyutich and K. Gusak, *Russ. J. Org. Chem.*, 2016, **52**, 139–177.
15 S. S. Ganguly and R. Plattner, *Genes Cancer*, 2012, **3**, 414–425.
16 S. A. Rosenzweig, *Adv. Cancer Res.*, 2018, **138**, 71–98.
17 J. V. Melo and C. Chuah, *Cancer Lett.*, 2007, **249**, 121–132.
18 V. Nardi, M. Azam and G. Q. Daley, *Curr. Opin. Hematol.*, 2004, **11**, 35–43.
19 A. Rahim, R. Syed, Y. Poornachandra, M. S. Malik, C. V. R. Reddy, M. Alvala, K. Boppana, B. Sridhar, R. Amanchy and A. Kamal, *Med. Chem. Res.*, 2019, **28**, 633–645.
20 J. Dietrich, C. Hulme and L. H. Hurley, *Bioorg. Med. Chem. Lett.*, 2010, **18**, 5738–5748.
21 J. Lee, K.-H. Kim and S. Jeong, *Bioorg. Med. Chem. Lett.*, 2011, **21**, 4203–4205.
22 K. P. Cheremnykh, V. A. Savelyev, M. A. Pokrovskii, D. S. Baev, T. G. Tolstikova, A. G. Pokrovskii and E. E. Shults, *Med. Chem. Res.*, 2019, **28**, 545–558.
23 R. Ramajayam, R. Giridhar, M. R. Yadav, H. Djaballah, D. Shum and C. Radu, *J. Enzyme Inhib. Med. Chem.*, 2007, **22**, 716–721.
24 F. Giraud, G. Alves, E. Debiton, L. Nauton, V. Théry, E. Durieu, Y. Ferandin, O. Lozach, L. Meijer and F. Anizon, *J. Med. Chem.*, 2011, **54**, 4474–4489.

25 F. Jubeen, S. Z. Iqbal, N. Shafiq, M. Khan, S. Parveen, M. Iqbal and A. Nazir, *Synth. Commun.*, 2018, **48**, 601–625.
26 S. Wang, X.-H. Yuan, S.-Q. Wang, W. Zhao, X.-B. Chen and B. Yu, *Eur. J. Med. Chem.*, 2021, **214**, 113218.
27 I. M. Lagoja, *Chem. Biodiversity*, 2005, **2**, 1–50.
28 S. A. Rostom, M. H. Badr, H. A. A. E. Razik, H. M. Ashour and A. E. A. Wahab, *Arch. Pharm.*, 2011, **344**, 572–587.
29 S. Farooq and Z. Ngaini, *J. Heterocycl. Chem.*, 2021, **58**, 1209–1224.
30 N. Kahriman, K. Peker, V. Serdaroğlu, A. Aydın, A. Usta, S. Fandaklı and N. Yaylı, *Bioinorg. Chem.*, 2020, **99**, 103805.
31 A. E. Aiwonegbe, J. U. Iyasele and C. O. Usifoh, *ChemSearch J.*, 2024, **15**, 112–124.
32 S. Prasad, V. Radhakrishna and T. K. Ravi, *Arabian J. Chem.*, 2019, **12**, 3943–3947.
33 M. H. Ahmed, M. A. El-Hashash, M. I. Marzouk and A. M. El-Naggar, *J. Heterocycl. Chem.*, 2020, **57**, 3412–3427.
34 A. R. Dwivedi, V. Kumar, H. Kaur, N. Kumar, R. P. Yadav, R. Poduri, S. Baranwal and V. Kumar, *Bioorg. Med. Chem. Lett.*, 2020, **30**, 127468.
35 X. An, A. K. Tiwari, Y. Sun, P.-R. Ding, C. R. Ashby Jr and Z.-S. Chen, *Leuk. Res.*, 2010, **34**, 1255–1268.
36 T. Mosmann, *J. Immunol. Methods*, 1983, **65**, 55–63.
37 S. K. Burley, C. Bhikadiya, C. Bi, S. Bittrich, H. Chao, L. Chen, P. A. Craig, G. V. Crichlow, K. Dalenberg, J. M. Duarte, S. Dutta, M. Fayazi, Z. Feng, J. W. Flatt, S. Ganesan, S. Ghosh, D. S. Goodsell, R. K. Green, V. Guranovic, J. Henry, B. P. Hudson, I. Khokhriakov, C. L. Lawson, Y. Liang, R. Lowe, E. Peisach, I. Persikova, D. W. Piehl, Y. Rose, A. Sali, J. Segura, M. Sekharan, C. Shao, B. Vallat, M. Voigt, B. Webb, J. D. Westbrook, S. Whetstone, J. Y. Young, A. Zalevsky and C. Zardecki, *Nucleic Acids Res.*, 2023, **51**, D488–D508.
38 S. W. Cowan-Jacob, G. Fendrich, A. Floersheimer, P. Furet, J. Liebetanz, G. Rummel, P. Rheinberger, M. Centeleghe, D. Fabbro and P. W. Manley, *Acta Crystallogr., Sect. D:Biol. Crystallogr.*, 2007, **63**, 80–93.
39 K. A. Rygiel and J. M. Elkins, *Curr. Opin. Struct. Biol.*, 2023, **82**, 102665.
40 A. A. Wylie, J. Schoepfer, W. Jahnke, S. W. Cowan-Jacob, A. Loo, P. Furet, A. L. Marzinzik, X. Pelle, J. Donovan, W. Zhu, S. Buonamici, A. Q. Hassan, F. Lombardo, V. Iyer, M. Palmer, G. Berellini, S. Dodd, S. Thohan, H. Bitter, S. Branford, D. M. Ross, T. P. Hughes, L. Petruzzelli, K. G. Vanasse, M. Warmuth, F. Hofmann, N. J. Keen and W. R. Sellers, *Nature*, 2017, **543**, 733–737.
41 G. M. Morris, R. Huey, W. Lindstrom, M. F. Sanner, R. K. Belew, D. S. Goodsell and A. J. Olson, *J. Comput. Chem.*, 2009, **30**, 2785–2791.
42 O. Trott and A. J. Olson, *J. Comput. Chem.*, 2010, **31**, 455–461.
43 K. Stierand and M. Rarey, *ACS Med. Chem. Lett.*, 2010, **1**, 540–545.
44 D. A. Case, H. M. Aktulga, K. Belfon, I. Y. Ben-Shalom, J. T. Berryman, S. R. Brozell, D. S. Cerutti, T. E. Cheatham, G. A. Cisneros, V. W. D. Cruzeiro, T. A. Darden, N. Forouzesh, G. Giambaşu, M. K. T. Giese, H. G. Gilson, A. W. Goetz, J. Harris, S. Izadi, S. A. Izmailov, K. Kasavajhala, M. C. Kaymak, E. King, A. Kovalenko, T. Kurtzman, T. S. Lee, P. Li, C. Lin, J. Liu, T. Luchko, R. Luo, M. Machado, V. Man, M. Manathunga, K. M. Merz, Y. Miao, O. Mikhailovskii, G. Monard, H. Nguyen, K. A. O'Hearn, A. Onufriev, F. Pan, S. Pantano, R. Qi, A. Rahnamoun, D. R. Roe, A. Roitberg, C. Sagui, S. Schott-Verdugo, A. Shajan, J. Shen, C. L. Simmerling, N. R. Skrynnikov, J. Smith, J. Swails, R. C. Walker, J. Wang, J. Wang, H. Wei, X. Wu, Y. Wu, Y. Xiong, Y. Xue, D. M. York, S. Zhao, Q. Zhu and P. A. Kollman, **https://ambermd.org/**, Accessed September 2024.
45 T. T. Mai, T.-P. Lam, L.-H. D. Pham, K.-H. Nguyen, Q.-T. Nguyen, M.-T. Le and K.-M. Thai, *J. Phys. Chem. B*, 2024, **128**, 8362–8375.
46 D. R. Roe and T. E. Cheatham III, *J. Chem. Theory Comput.*, 2013, **9**, 3084–3095.
47 B. R. Miller, T. D. McGee, J. M. Swails, N. Homeyer, H. Gohlke and A. E. Roitberg, *J. Chem. Theory Comput.*, 2012, **8**, 3314–3321.
48 C. Bouysset and S. Fiorucci, *J. Cheminf.*, 2021, **13**, 72.
49 N. Michaud-Agrawal, E. J. Denning, T. B. Woolf and O. Beckstein, *J. Comput. Chem.*, 2011, **32**, 2319–2327.